MR of the Spine with a Fast T1-Weighted Fluid-Attenuated Inversion Recovery Sequence

Elias R. Melhem, David A. Israel, Steve Eustace, and Hernan Jara

PURPOSE: To optimize a T1-weighted fast fluid-attenuated inversion recovery (FLAIR) sequence using computer-simulated data and to study its clinical utility for imaging the spine. **METHODS:** Relative signal intensities and contrast of relevant normal and pathologic tissues in the spine were computed using an inversion recovery equation modified to account for a hybrid RARE (rapid acquisition with relaxation enhancement) readout. A range of inversion time (TI) and repetition time (TR) pairs that null the signal from CSF was generated. A contrast-optimized heavily T1-weighted fast FLAIR sequence, based on the generated data, was qualitatively compared with conventional T1-weighted spin-echo sequences for imaging various spinal abnormalities. **RESULTS:** A TI/TR pair of approximately 862/2000 was extracted from the computer-generated data to produce effective nulling of CSF signal, to achieve heavy T1 weighting, and to optimize contrast between abnormal tissues and cord/bone marrow. Clinical implementation of the optimized T1-weighted fast FLAIR sequence revealed superior contrast at the CSF-cord interface, better conspicuity of lesions of the spinal cord and bone marrow, and reduced hardware-related artifacts as compared with conventional T1-weighted spin-echo sequences. **CONCLUSION:** The optimized T1-weighted fast FLAIR technique has definite advantages over spin-echo sequences for imaging the spine. Comparable acquisition times render the FLAIR sequence the method of choice for T1-weighted imaging of the spine.

Index terms: Spine, magnetic resonance; Magnetic resonance, technique

AJNR Am J Neuroradiol 18:447–454, March 1997

Fluid-attenuated inversion recovery (FLAIR) magnetic resonance (MR) imaging techniques have been described by Hajnal et al (1, 2). Cerebrospinal fluid (CSF) nulling allowed the use of long echo time (TE) readout (increased T2 weighting), hence improving the conspicuity of most tissue abnormalities without the deleterious effects of CSF artifacts and volume averaging seen on conventional T2-weighted spin-echo (SE) sequences (3). Despite the success of T2-weighted FLAIR sequences in displaying lesions not detected on conventional T2-weighted SE images (4), their clinical utility has been limited by long acquisition times (in excess of 12 minutes). To improve imaging efficiency and clinical utility, technical refinements, such as rapid acquisition with relaxation enhancement (RARE) and sequential interleaving, were incorporated in the basic FLAIR sequence (3, 5, 6).

Recently, Bydder and Young (7) and Rydberg et al (8) have described a fast T1-weighted inversion recovery (IR) sequence that coupled an IR preparation pulse to a hybrid-RARE readout. This sequence produced superior gray-to-white-matter contrast and improved lesion-to-background contrast in the brain as compared with conventional T1-weighted SE sequences.

In this work, we present a theoretical signal intensity (SI) analysis of fatty marrow, white matter, gray matter, and abnormal tissues using a T1-weighted hybrid-RARE FLAIR technique. Different relatively short repetition time (TR) and inversion time (TI) pairs were selected to null CSF and to vary T1 effects of non-CSF tissues on the desired signal intensities. The

Received July 3, 1996; accepted after revision September 30.

Supported in part by a research grant from Philips Medical Systems.

From the Department of Radiology, Boston University Medical Center, 88 E Newton St, Atrium 2, Boston, MA 02118. Address reprint requests to Elias R. Melhem, MD.

AJNR 18:447–454, Mar 1997 0195-6108/97/1803–0447

clinical utility of this fast T1-weighted FLAIR sequence for spinal imaging was evidenced with regard to cord (cauda equina)–CSF interface, cord and marrow abnormalities, nucleus pulposus (inner annulus fibrosus)–outer annulus fibrosus differentiation, and image artifacts from metallic hardware.

Materials and Methods

Theoretical Analysis

The SI in an IR sequence performed with a hybrid-RARE readout is approximated by the following equation:

$$1) \quad SI = K[1 - 2e^{-TI/T1} + e^{-(TR-TElast)/T1}]e^{-TEeff/T2} \quad (9)$$

where K is proportional to the specific tissue proton density (ρ) and is related to voxel size, data sampling period, number of phase-encoding steps, number of excitations, and magnetic field strength. The TE_{eff} and the TE_{last} are the effective echo time and the time of the last echo in a hybrid-RARE readout, respectively. The T1 and T2 are the tissue-specific longitudinal and transverse relaxation times, respectively. In the computer-generated data to follow, the TE_{eff} was 10 milliseconds, thus minimizing the T2 effects of tissues on SI, and the TE_{last} was 60 milliseconds (echo train length of six and echo spacing of 10 milliseconds).

To null the SI of a specific tissue (SI_x), the term in parentheses in Equation 1 was equated to zero:

$$2) \quad [1 - 2e^{-TI/T1} + e^{-(TR - TElast)/T1}] = 0.$$

From Equation 2 an expression can be derived that relates the null TI_x of a specific tissue to the TR, $T1_x$, and TE_{last} (note, the latter is fixed at 60 milliseconds):

$$\text{null } TI_x = T1_x[\ln 2 - \ln(1 + e^{-(TR - TElast)/T1x})]$$

$$3) \quad \text{or}$$

$$\text{null } TI_x = T1_x[\ln 2 - \ln(1 + e^{-(TR - 60)/T1x})].$$

Using Equation 3, the null TI of CSF was calculated as a function of TR (range, 500 to 5000) (Fig 1). Approximate values of T1 for CSF were used (Table).

Using Equation 1, SIs of relevant tissues in spine imaging (fatty marrow, white matter, gray matter, and abnormal tissue with T1 and T2 relaxation times longer than gray matter) were calculated at different CSF-nulling TI/TR pairs (Fig 2). Approximate T1 and T2 relaxation times and ρ values of the different tissues were used in the calculations (Table). The voxel size, data sampling period, number of phase-encoding steps, number of excitations, and magnetic field strength were assumed fixed and assigned a normalized value of 1. From the computer-generated SIs, fatty marrow–abnormal tissue contrast ($SI_{fatty\ marrow} - SI_{abnormal\ tissue}$), white matter–abnormal tissue contrast ($SI_{white\ matter} - SI_{abnormal\ tissue}$), and white matter–gray matter contrast ($SI_{white\ matter} - SI_{gray\ matter}$) were calculated at different CSF-nulling TI/TR pairs (Fig 3).

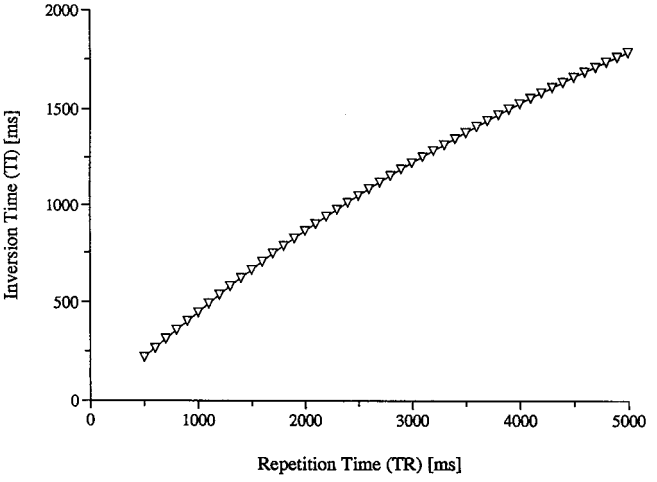

Fig 1. Plot of TI versus TR of the modified FLAIR sequence. TI was calculated (Equation 3) to null signal from CSF at different TRs (assumed $T1_{CSF}$ is 4210 milliseconds).

Approximate relaxation times and proton densities (ρ) at 1.5 T for human tissues*

Tissue	T1, ms	T2, ms	ρ (Relative to CSF)
Gray matter	940	100	0.75
White matter	550	90	0.65
Fat (yellow marrow)	260	84	1.0
CSF	4210	2100	1.0
Lesion (abnormal tissue)†	1300	150	0.80

* See Rydberg et al (9), Brix et al (21), and Bottomley et al (22).
† Reported mean values for multiple sclerosis plaques (9).

Fast T1-Weighted FLAIR Sequence

A commercially available hybrid-RARE readout, implementing an echo-to-view mapping scheme, termed "low-high profile order," was incorporated in a T1-weighted FLAIR sequence. This mapping scheme was designed to achieve the shortest possible effective echo times, hence minimizing T2 effects. The lower-order phase-encoded lines were acquired at the beginning of the echo train, while the higher-order lines were acquired at later times in an alternating fashion (Fig 4). Furthermore, in each shot, the successive profiles were closely packed, separated in time by an echo spacing equal in value to the TE_{eff} (10 milliseconds). An echo train length of six was used to improve the section/time efficiency of the T1-weighted FLAIR sequence. Image degradation resulting from phase-encode noise and blurring was minimal at this echo train length (10).

A relatively short CSF-nulling TI/TR pair was chosen to optimize fatty marrow–abnormal tissue contrast and white matter–abnormal tissue contrast (Fig 3) and to maintain strong T1 weighting (TI and the postsampling signal recovery delay [approximately TR − TI − TE] would be

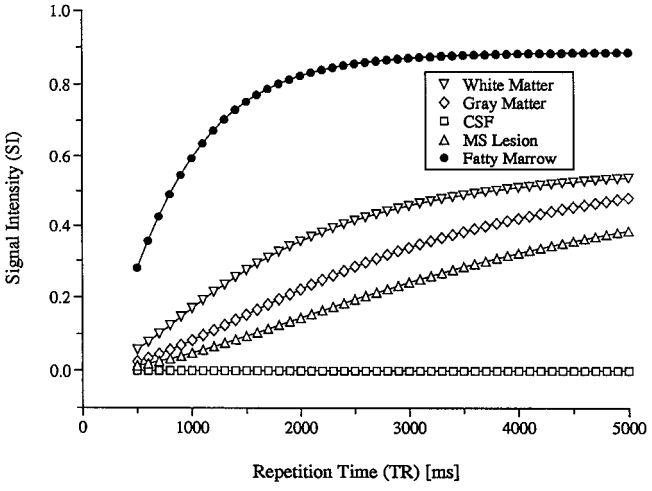

Fig 2. Plot of relative SI from fatty marrow, white matter, gray matter, CSF, and abnormal tissue versus CSF-nulling TI/TR pairs. The SIs were calculated for different tissues (Table) using Equation 1. Of the CSF-nulling TI/TR pairs, only the TR values appear on the *x*-axis.

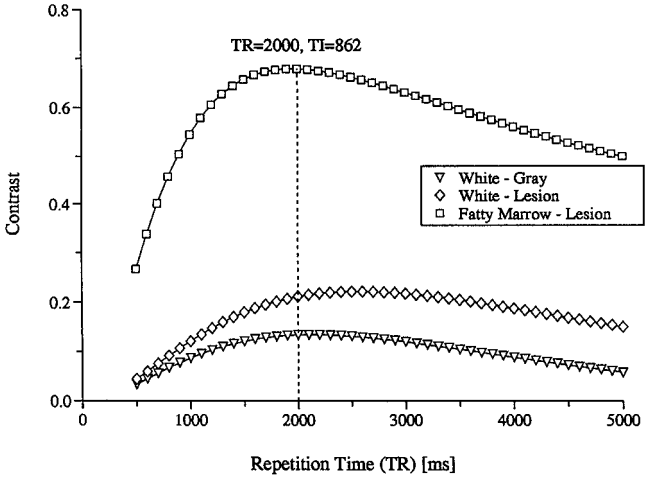

Fig 3. Plot of contrast ($SI_x - SI_y$): fatty marrow–abnormal tissue, white matter–abnormal tissue, and white matter–gray matter versus CSF-nulling TI/TR pairs. Contrast between different tissues was calculated using data from Figure 2. The CSF-nulling TI/TR pair (862/2000) responsible for peak fatty marrow–abnormal tissue contrast and near peak white matter–abnormal tissue and white matter–gray matter contrast was chosen for the clinical study.

between one and two times the T1 of white matter [approximately 1000 milliseconds]).

The remaining parameters of the fast T1-weighted FLAIR sequence were identical to the conventional sagittal T1-weighted SE cervical spine imaging protocol used at our institution: four excitations; 240-mm (75% rectangular) field of view; 200 × 256 matrix (phase encoding in the anteroposterior direction); 3.0-mm section thickness; 0.3-mm intersection gap; 11 sections; and ±32 kHz receiver bandwidth. The total scan time varied from 5 to 6 minutes depending on the TR used. Minor parameter

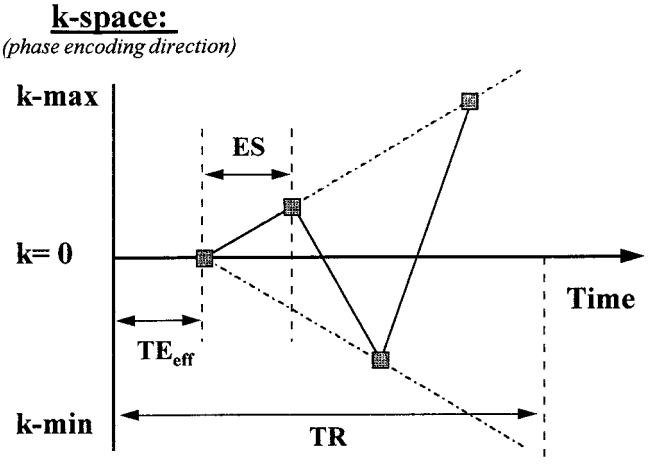

Fig 4. "Low-high profile order" echo-to-view mapping scheme used in the T1-weighted fast FLAIR sequence.

changes were made relative to the region (cervical versus thoracic versus lumbosacral) and plane of interest.

Patients' Studies

All examinations were performed on 1.5-T, 10, and 15 mT/m MR systems. Quadrature neck and phase-array surface coils were used depending on the region of interest. Twenty consecutive patients with a spectrum of spinal abnormalities, including multiple sclerosis, metastatic disease, degenerative disease, syrinx, trauma, and metallic fusion, were imaged with a conventional T1-weighted SE sequence and a fast T1-weighted FLAIR sequence, matched for spatial resolution and receiver bandwidth. The images from the two sequences, filmed at optimal window and level settings, were compared by two neuroradiologists using five qualitative criteria: 1) lesion conspicuity in spinal cord and bone marrow; 2) contrast at the cord (cauda equina)–CSF interface; 3) contrast at the disk-CSF interface; 4) contrast at the nucleus pulposus (inner annulus fibrosus)–outer annulus fibrosus interface; and 5) image artifacts, especially those pertaining to ghosting and blurring along the phase-encoding direction as well as to metallic hardware. A score of 1 to 3 (1 being the worst) was assigned by the two observers for the different qualitative criteria in each case. The scores were analyzed by means of a Wilcoxon's ranked-order test.

Results

Theoretical Analysis

Figure 1 plots the null TI of CSF versus TR (500 to 5000) using Equation 3, and Figure 3 plots fatty marrow–abnormal tissue contrast ($SI_{fatty\ marrow} - SI_{abnormal\ tissue}$), white matter–abnormal tissue contrast ($SI_{white\ matter} - SI_{abnormal\ tissue}$), and white matter–gray matter

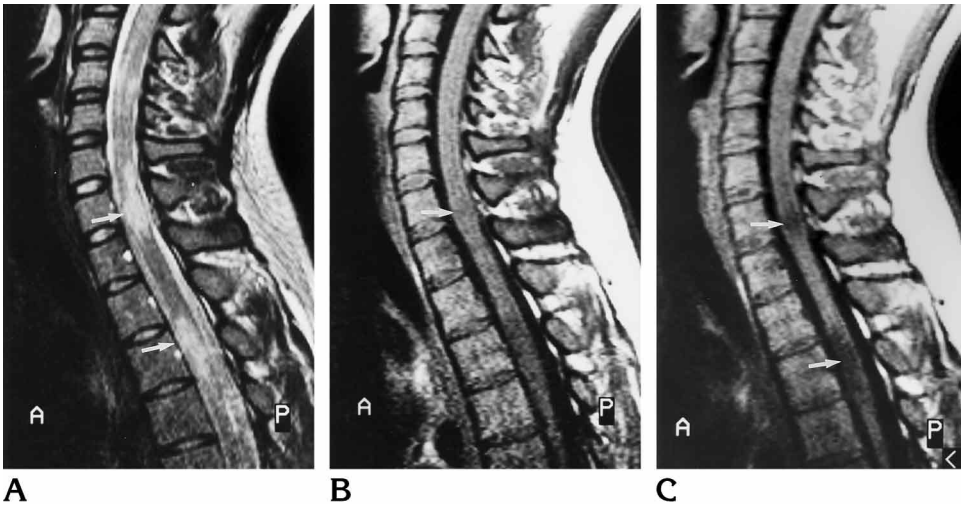

Fig 5. A 28-year-old woman with multiple sclerosis.

A, Sagittal fast SE T2-weighted image (2800/90/4 [TR/effective TE/excitations], echo train length of 16) of the cervical spine shows two hyperintense lesions involving the spinal cord (*arrows*).

B, On sagittal T1-weighted SE image (500/20/4) of the cervical spine, the upper lesion is poorly seen (*arrow*) and the lower lesion is inconspicuous.

C, On the T1-weighted fast FLAIR sequence (2000/10 effective/4, TI of 862, echo train length of six), both lesions were easily appreciated (*arrows*).

contrast ($SI_{white\ matter} - SI_{gray\ matter}$) versus CSF-nulling TI/TR pairs. From these plots we extracted a TI/TR pair of approximately 862/2000 to fulfill the following three objectives: nulling of CSF, achieving T1 weighting, and optimizing contrast between abnormal tissues and cord/fatty marrow.

Patients' Studies

A total of 20 patients were imaged using a conventional T1-weighted SE (500/20/4 [TR/TE/excitations]) sequence and a fast T1-weighted FLAIR (2000/10/4, TI of 862) sequence. Three had multiple sclerosis plaques involving the cervical spine, three had compression fractures involving the lumbar or cervical spine, two had syrinxes involving the cervical spine, one had a decompressed peritumoral cyst and edema involving the cervical cord, two had metastatic lesions to the cervical and lumbar spine from breast and renal cell carcinoma, respectively, six had spondylitic disease of the cervical or lumbar spine, and three had anterior fusion of the cervical spine with metallic hardware (Figs 5–10).

Effective nulling of CSF signal was achieved in all imaged patients; the mean signal-to-noise ratio (S/N) of CSF was 0.6 for the T1-weighted FLAIR sequence as compared with a mean S/N_{CSF} of 39.2 for the T1-weighted SE sequence. The lesion conspicuity score was significantly higher ($P < .01$) for the fast T1-weighted FLAIR sequence (Figs 5–8). Contrast scores for the cord (cauda equina)-CSF interface, the disk-CSF interface, and the nucleus pulposus (inner annulus fibrosus)–outer annulus fibrosus interface were also significantly higher ($P < .001$) for the fast FLAIR sequence, most evident at levels of spinal stenosis related to spondylitic disease (Fig 9). Differentiation between the nucleus pulposus (inner annulus fibrosus) and outer annulus fibrosus was better on the fast FLAIR sequence (Figs 6 and 9). The difference in the image artifact scores (excluding patients with metallic hardware in place) between the two techniques was not significant ($P > .05$). There was a moderate reduction of

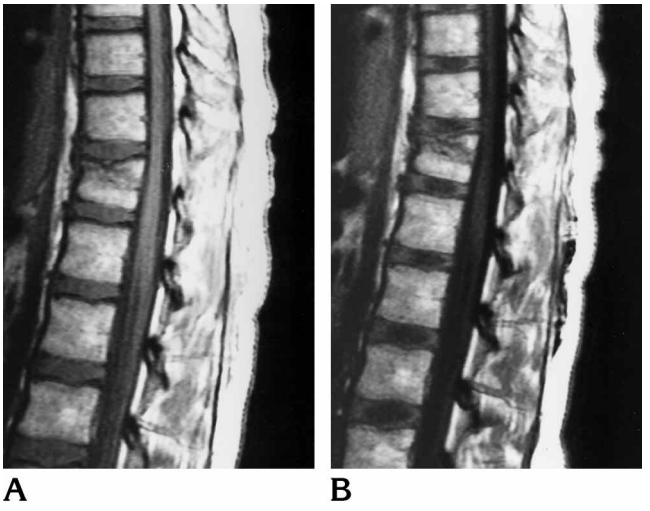

Fig 6. A 20-year-old woman involved in a motor vehicle accident.

Both the sagittal T1-weighted SE (500/20/4) image (*A*) and the sagittal T1-weighted fast FLAIR (2000/10 effective/4, TI of 862, echo train length of six) image (*B*) showed a compression fracture of the T-11 vertebral body with edema partially replacing the marrow. Note greater contrast between the edema and marrow and better differentiation between the nucleus pulposus (inner annulus fibrosus) and outer annulus fibrosus of the disks on the FLAIR sequence.

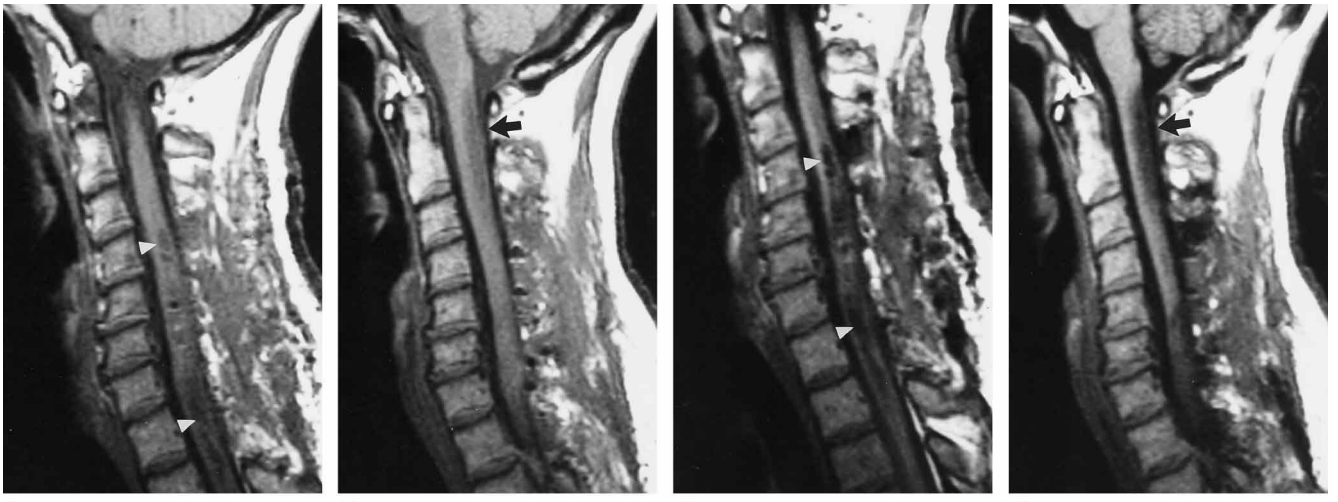

Fig 7. A 46-year-old woman after resection of an intramedullary ependymoma involving the cervical spine with decompression of a peritumoral cyst.

Note that the decompressed cyst (*arrowheads* in *A* and *C*) and the cord edema (*arrows* in *B* and *D*) are less conspicuous on the sagittal T1-weighted SE (500/20/4) sequences (*A* and *B*) than on the T1-weighted fast FLAIR (2000/10 effective/4, TI of 862, echo train length of 6) sequences (*C* and *D*). Note also the improved gray–white matter differentiation in the cerebellum on the fast FLAIR sequence.

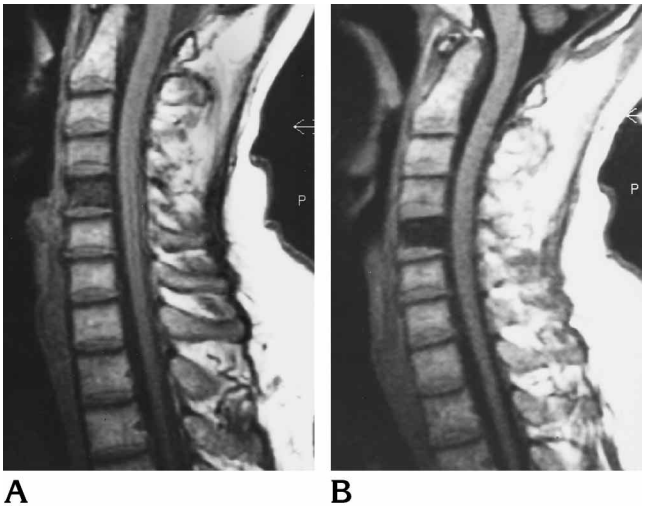

Fig 8. A 53-year-old woman with metastatic breast cancer.

Both the sagittal T1-weighted SE (500/20/4) (*A*) and the sagittal T1-weighted fast FLAIR (2000/10 effective/4, TI of 862, echo train length of 6) (*B*) sequences showed a low-SI lesion completely replacing the marrow of the C-5 vertebral body, consistent with metastases. Note the greater contrast between the lesion and marrow and less internal detail of the vertebral body on the FLAIR sequence.

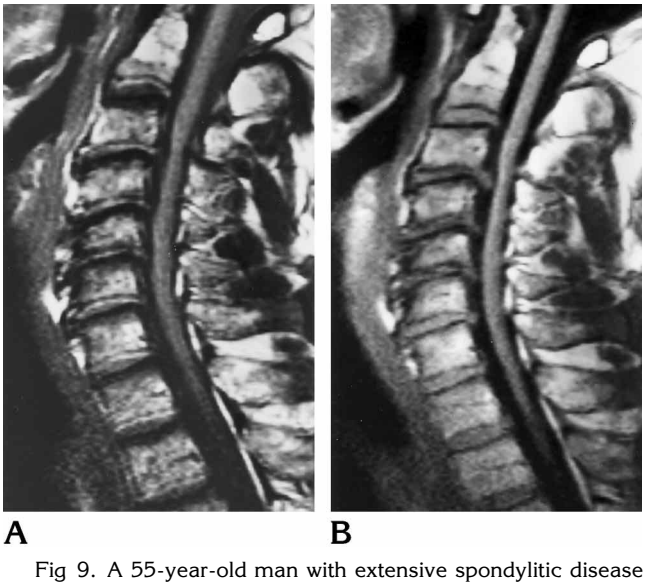

Fig 9. A 55-year-old man with extensive spondylitic disease of the cervical spine.

Note that the disk-CSF and cord-CSF contrast is less on the sagittal T1-weighted SE (500/20/4) image (*A*) than on the sagittal T1-weighted fast FLAIR (2000/10 effective/4, TI of 862, echo train length of six) image (*B*). Note better visibility of the internal architecture of the disks on the FLAIR sequence.

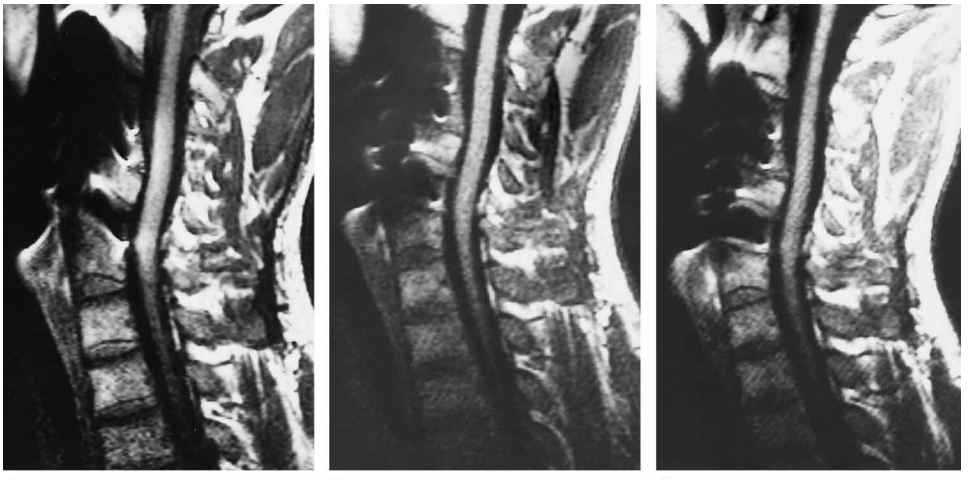

Fig 10. A 34-year-old man with anterior fusion (metallic hardware and bone graft) of the cervical spine who was being examined for the presence of a posttraumatic syrinx.

Note gradual decrease in the hardware-related artifact along the frequency-encoding (craniocaudal) and phase-encoding (anteroposterior) directions from the sagittal T1-weighted SE (500/20/4) image (*A*) to the sagittal T1-weighted fast FLAIR (2000/10 effective/4, TI of 862, echo train length of 6) image (*B*) to the sagittal T1-weighted fast FLAIR (2000/10 effective/4, TI of 862, echo train length of 10) (*C*) image, leading to improved delineation of the individual screws with higher echo train length. This reduction in hardware-related artifact with increased echo train length (at fixed echo spacing of 10 milliseconds) is limited by worsening corduroy artifact related to spikes in raw data, image ghosting, and blurring (*C*).

paramagnetic susceptibility artifacts from metallic hardware on the fast FLAIR sequence as compared with the conventional SE sequence (Fig 10).

Discussion

In the past, the clinical utility of IR sequences was limited by long acquisition times. The incorporation of a hybrid-RARE readout (echo train length of six) to our FLAIR technique was instrumental in improving section/time efficiency by a factor of six. This hybrid-RARE readout implemented an echo-to-view mapping scheme that was different from the mapping scheme used in the fast T2-weighted FLAIR sequences described (3). Specifically, the acquisition of lower-order phase-encoded lines in k-space occurred at the beginning of the echo train, permitting a short effective TE (10 milliseconds). However, the acquisition of the outer lines at later echo times in an alternating fashion rendered this echo-to-view mapping scheme susceptible to phase-encoding ghosting and blurring artifacts. With this particular phase-encoding reordering scheme, the severity of these artifacts was related to the echo train length and the T2 relaxation times of tissues imaged (10). Using an echo train length of six, the imaging efficiency of the T1-weighted FLAIR became comparable to that of the conventional T1-weighted SE sequence and at the same time limited image artifacts.

Another advantage of incorporating a hybrid-RARE readout to the FLAIR sequence is the reduction of paramagnetic susceptibility artifacts induced by metallic hardware (Fig 10). Signal losses due to local magnetic field inhomogeneity induced by paramagnetic substances can be limited by the application of multiple refocusing 180° radio frequency pulses (echo train) (11). The number of refocusing pulses (echo train length) that can be applied, however, is limited by phase-encoding ghosting and blurring artifacts (Fig 10).

Fast T1-weighted (short TI) IR sequences have been achieved at relatively longer TRs as compared with T1-weighted FLAIR sequences, thus improving S/N (8). Our choice of a TI/TR pair was dictated by two conditions: CSF nulling and optimization of fatty marrow–abnormal tissue contrast and white matter–abnormal tissue contrast (Figs 1 and 2). A relatively short TR (approximately 2000 milliseconds) was necessary to obtain CSF nulling at a short TI (similar to the T1 of white matter) (Fig 1). The second condition was used to optimize our TI/TR pair selection. This short TR selection alone would result in S/N loss in our fast FLAIR sequence. However, the implementation of the hybrid-RARE readout enabled an increased number of excitations (four), compensating for theoretical S/N loss without limiting the clinical utility of the sequence (total scan time, 5 to 6 minutes).

The advantages of nulling CSF were demonstrated by improved conspicuity of syrinxes and

cord cysts, as well as by better contrast at the CSF-cord and CSF-disk interfaces (Figs 7 and 9). This resulted in improved differentiation between syrinx and myelomalacia. Other advantages may include improved detection and/or conspicuity of enhancing CSF drop metastases and intradural epidermoids (characteristic long T1 and T2). Further, the short TR increased the T1 weighting of the fast FLAIR sequence by reducing the postsampling signal recovery delay (approximately TR − TI − TE). A subsequent benefit was the improved conspicuity of edema and metastatic lesions in the fatty marrow (Figs 6 and 8). The expected broader dynamic contrast range of IR sequences, as compared with SE sequences, was well seen on the T1-weighted FLAIR images of patients with multiple sclerosis (Fig 5).

In our study, the computer-generated data regarding CSF-nulling TI/TR pairs (Fig 1) and SIs of relevant tissues (Fig 2) had certain limitations. Although the modified IR equation (Equation 1) used accounted for the incorporation of the hybrid-RARE readout, it did not address the potential effects of the echo-to-view mapping scheme on the SIs of different tissues. Further, the development of this equation did not consider the effects of stimulated echoes and of magnetization transfer inherent to hybrid-RARE techniques (11–13). Inherent magnetization transfer effects are dependent on the number of sections per TR, the total power applied off-resonance (related to the number of 180° radio frequency pulses applied in rapid succession: echo train length), the time between application of these off-resonance pulses and acquisition of signal from the section of interest, and both linewidth and shape of the tissue's broad proton component (11). Owing to the paucity of macromolecules in CSF, the generated CSF-nulling TI/TR pairs were minimally affected by magnetization transfer effects in fast FLAIR sequences (14–16). However, magnetization transfer-active tissues (ie, spinal cord) may have significant alterations in their SIs (17). The recent increased clinical utility of these hybrid-RARE FLAIR techniques necessitates further experimental and theoretical investigations to define potential effects of various fast imaging techniques on the generated signal.

Further limitations of our results were related to the estimated T1, T2, and ρ values used to calculate tissue SI. It has been well documented that the relative concentrations of hematopoietic cells, fat, and bone in bone marrow vary with age and medical conditions (such as acquired immunodeficiency syndrome, aplastic anemia, myelofibrosis, hemoglobinopathies, and infiltrative neoplasms) (18–20). Thus, using the relaxation times of fat as representatives of bone marrow, although practical, was somewhat crude. Also, T1, T2, and ρ values of abnormal tissues within bone marrow and spinal cord vary depending on the histopathologic nature of the process. Published values for multiple sclerosis were thought to represent abnormal tissue adequately for this theoretical analysis (9). Finally, the SI of tissue varies with voxel size, data sampling period, number of phase-encoding steps, number of excitations, and magnetic field strength. In our calculations, these variables were assumed fixed and their composite effect was normalized. Although this most likely has an effect on the absolute value of the calculated SI, it should have no effect on the relative values and hence on the calculated tissue contrast as a function of CSF-nulling TI/TR pairs (Fig 3).

Finally, the two T1-weighted sequences compared in our study had different echo times (10 milliseconds for the TE_{FLAIR} sequence versus 20 milliseconds for TE_{SE}). An extra T1-weighted SE sequence with a TE of 10 milliseconds was not implemented because of time constraints. However, this difference in echo time has a negligible effect on SI ($\alpha\ e^{-TE/T2}$) from the tissues under evaluation, especially since the T2 relaxation times of all the tissues considered are much greater than the TE and effective TE used.

In conclusion, optimized T1-weighted fast FLAIR imaging of the spine provides improved conspicuity of abnormal tissues in the bone marrow and spinal cord, better contrast at the CSF-cord interface and the nucleus pulposus (inner annulus fibrosis)–outer annulus fibrosis interface, and diminished hardware-related artifacts as compared with conventional T1-weighted SE techniques. The incorporation of a hybrid-RARE readout is pivotal in making the acquisition time of the T1-weighted FLAIR sequence similar to that of a conventional T1-weighted SE technique. Further experimental and theoretical investigations are needed to define better the effects of various fast imaging techniques on the signal generated by conventional IR sequences.

References

1. Hajnal JV, Bryant DJ, Kasuboski L, et al. Use of fluid-attenuated inversion recovery (FLAIR) pulse sequences in MRI of the brain. *J Comput Assist Tomogr* 1992;16:841–844
2. White SJ, Hajnal JV, Young IR, et al. Use of fluid-attenuated inversion recovery pulse sequences for imaging the spinal cord. *Magn Reson Med* 1992;28:153–162
3. Rydberg JN, Hammond CA, Grimm RC, et al. Initial clinical experience in MR imaging of the brain with a fast fluid attenuated inversion-recovery pulse sequence. *Radiology* 1994;193: 173–180
4. De Coene B, Hajnal JV, Gatehouse P, et al. MR of the brain using fluid-attenuated inversion recovery (FLAIR) pulse sequences. *AJNR Am J Neuroradiol* 1992;13:1555–1564
5. Park HW, Cho MH, Cho ZH. Time-multiplexed multi-slice inversion-recovery techniques for NMR imaging. *Magn Reson Med* 1985;2:534–539
6. Stehling MK, Ordidge RJ, Coxon R, et al. Inversion-recovery echo-planar imaging (IR-EPI) at 0.5 T. *Magn Reson Med* 1990;13:514–517
7. Bydder GM, Young IR. MR imaging: clinical use of the inversion recovery sequence. *J Comput Assist Tomogr* 1985;9:659–675
8. Rydberg JN, Hammond, Huston J III, et al. T1-weighted MR imaging of the brain using a fast inversion recovery pulse sequence. *J Magn Reson Imaging* 1996;6:356–362
9. Rydberg JN, Riederer SJ, Rydberg CH, et al. Contrast optimization of fluid-attenuated inversion recovery (FLAIR) imaging. *Magn Reson Med* 1995;34:868–877
10. Melki PS, Jolesz FA, Mulkern RV. Partial RF echo planar imaging with the FAISE method, I: experimental and theoretical assessment of artifact. *Magn Reson Med* 1992;26:328–341
11. Constable RT, Anderson AW, Zhong J, Gore JC. Factors influencing contrast in fast spin-echo MR imaging. *Magn Reson Imaging* 1992;10:497–511
12. Melki PS, Mulkern RV. Magnetization transfer effects in multislice RARE sequences. *Magn Reson Med* 1992;24:189–195
13. Melki PS, Jolesz FA, Mulkern RV. Partial RF echo planar imaging with the FAISE method, II: contrast equivalence with spin-echo sequences. *Magn Reson Med* 1992;26:342–354
14. Dousset V, Grossman RI, Ramer KN, et al. Experimental allergic encephalomyelitis and multiple sclerosis: lesion characterization with magnetization transfer imaging. *Radiology* 1992;182:483–491
15. Eng J, Ceckler TL, Balaban R. Quantitative ^{1}H magnetization transfer in vivo. *Magn Reson Med* 1991;17:304–314
16. Wolff SD, Balaban RS. Magnetization transfer contrast (MTC) and tissue water proton relaxation in vivo. *Magn Reson Med* 1989;10: 135–144
17. Melhem ER, Benson ML, Beauchamp NJ, et al. Cervical spondylosis: three-dimensional gradient-echo MR with magnetization transfer. *AJNR Am J Neuroradiol* 1996;17:705–711
18. Custer RP, Ahlfeldt FE. Studies on the structure and function of bone marrow. *J Lab Clin Med* 1932;17:951–960
19. Vogler JB III, Murphy WA. Bone marrow imaging. *Radiology* 1988;168:679–693
20. Mitchell DG, Burk DL Jr, Vinitski S, et al. The biophysical basis of tissue contrast in extracranial MR imaging. *AJR Am J Roentgenol* 1987;149:831–837
21. Brix G, Schad LR, Deimling M, et al. Fast and precise T1 imaging using a TOMROP sequence. *Magn Reson Imaging* 1990;8:351–356
22. Bottomley PA, Hardy CJ, Argersinger RE, et al. A review of ^{1}H nuclear magnetic resonance relaxation in pathology: are T1 and T2 diagnostic? *Med Phys* 1987;14:1–37